Regional variations in the diffusion of triggered seismicity

Regional variations in the diffusion of triggered seismicity

Conor McKernon and Ian G. Main
School of GeoSciences, University of Edinburgh, Edinburgh, UK

Received 15 August 2004; revised 11 March 2005; accepted 25 March 2005; published 12 May 2005.

[1] We determine the spatiotemporal characteristics of interearthquake triggering in the International Seismological Centre catalogue on regional and global scales. We pose a null hypothesis of spatially clustered, temporally random seismicity, and determine a residual pair correlation function for triggered events against this background. We compare results from the eastern Mediterranean, 25 Flinn-Engdahl seismic regions, and the global data set. The null hypothesis cannot be rejected for distances greater than ~150 km, providing an upper limit to triggering distances that can be distinguished from temporally uncorrelated seismicity in the stacked data at present. Correlation lengths L and mean distances between triggered events $\langle r \rangle$ are on the order of 10–50 km, but can be as high as 100 km in subduction zones. These values are not strongly affected by magnitude threshold, but are comparable to seismogenic thicknesses, implying a strong thermal control on correlation lengths. The temporal evolution of L and $\langle r \rangle$ is well fitted by a power law, with an exponent $H \sim 0.1 \pm 0.05$. This is much lower than the value $H = 0.5$ expected for Gaussian diffusion in a homogenous medium. We observe clear regional variations in L, $\langle r \rangle$ and H that appear to depend on tectonic setting. A detectable transition to a more rapid diffusion regime occurs in some cases at times greater than 100–200 days, possibly due to viscoelastic processes in the ductile lower crust.

Citation: McKernon, C., and I. G. Main (2005), Regional variations in the diffusion of triggered seismicity, *J. Geophys. Res.*, *110*, B05S05, doi:10.1029/2004JB003387.

1. Introduction

[2] A triggered earthquake has been defined by *Gomberg et al.* [1998, p. 24,411] as "one whose failure time has been advanced by Δt (clock advance) due to a stress perturbation." This broad definition includes aftershocks, foreshocks, and induced seismicity, all normally defined at short range (within a few source dimensions) and, more rarely, longer-range triggered events. Importantly, it makes no retrospective judgment on what is a "main shock," since an individual earthquake may trigger subsequent larger events.

[3] Earthquake triggering is most evident in the spatial and temporal clustering of events in earthquake catalogues where the background seismicity is low. A high degree of temporal clustering of seismicity, especially in aftershock sequences [*Utsu et al.*, 1995], has long been recognized, but the spatial limits of more generally triggered events are still very much open to debate. One of the main reasons is the need to define an objective and robust "background" seismicity that would be expected for a temporally random (stationary) process, to act as a null hypothesis.

[4] Several authors have recently solved this problem, providing evidence for long-range triggering in the form of spatial and temporal clustering of seismicity outside the traditional "aftershock zone." *Lomnitz* [1996] suggested that triggered events were more likely to occur in two regions: (1) within 200 km of a main shock and (2) in an annulus of radii 300–1000 km over a 30 day period. *Gasperini and Mulargia* [1989] reported an aftershock "influence region" of 80–140 km, in a time window of 14–60 days. Evidence for triggering at distances up to 240 km was reported by *Parsons* [2002], with aftershocks occurring for 7–11 years. *Brodsky et al.* [2003] proposed that well water level changes could be linked to earthquakes hundreds of kilometers away, suggesting a very long range poroelastic mechanism. In contrast, *Melini et al.* [2002] found no strong statistical evidence for triggering at distances of several hundred kilometers.

[5] The precise mechanisms for triggering remain the subject of debate. One hypothesis is that earthquake triggering is caused by static Coulomb stress changes, where optimally orientated faults are brought closer to failure by stress redistribution after the triggering event. This view is supported by a wide literature of individual case studies [*King et al.*, 1994; *Stein et al.*, 1994; *Harris et al.*, 1995; *Harris and Simpson*, 1998; *Toda et al.*, 1998]. However, the more general effectiveness of Coulomb modeling as a predictive tool for zones of enhanced or reduced seismicity has recently come into question, based on statistical studies of the directional effect of triggering. For example, studies of global seismicity using centroid moment tensor (CMT) data [*Kagan and Jackson*, 1998; *Huc and Main*, 2003] demonstrate that shallow aftershocks do not necessarily concentrate preferentially in the dilatational quadrant. In a systematic statistical study of 100 large events, *Parsons*

0148-0227/05/2004JB003387$09.00

[2002] found that only 61% of aftershocks occurred in areas predicted to have increased Coulomb shear stress.

[6] The second hypothesis for triggered events (particularly at longer range) is dynamic stresses, which decay much more slowly with distance than static ones. A classical example of dynamic triggering is the observation of clearly triggered events in hydrothermal areas, beginning at or shortly after the passage of Raleigh waves propagated from the Landers earthquake [*Hill et al.*, 1993]. The most likely mechanism of triggering in such areas is the dynamic degassing of hydrothermal fluids and associated rapid increase in pore pressure.

[7] Whatever the primary mechanism, there is a clear time-dependant component to triggering, variously ascribed to pore fluid pressure changes, rate and state friction, stress corrosion cracking, and viscoelastic relaxation through a ductile lower crust. The relative importance of each is still open to question. For example, *Harris and Simpson* [1998] found that Coulomb stress calculations can in some cases predict stress shadows (areas of seismicity decrease) adequately, but require an explicit time-dependent effect (citing rate- and state-dependent friction) to achieve more accurate models.

[8] Additional complexity can be introduced through secondary triggering processes. For example, *Felzer et al.* [2002, 2003] suggested that the 1999 M_w 7.3 Hector Mine earthquake was triggered by aftershocks of the 1992 M_w 7.1 Landers earthquake. They propose that chains of cascading seismicity like this are part of the reason for the large proportion of observed discrepancies in statistical studies of Coulomb modeling. Although directly triggered aftershocks may be constrained to areas where a main shock increases shear stress, secondary aftershocks (aftershocks of aftershocks) can occur outside this area. *Felzer et al.* [2004] also suggest that the magnitude of each triggered earthquake may even be entirely independent of the magnitude of the triggering earthquake.

[9] *Marsan* [2003] puts forward a similar argument to *Felzer et al.* [2002, 2003] that positive triggering (i.e.; in areas of calculated Coulomb stress increase) is commonly observed, but seismic quiescence (in calculated "shadow zones" of Coulomb stress decrease) is less frequent. He suggests that high spatial variability of stresses caused by a main shock may explain the absence of quiescence (which static Coulomb modeling in a homogeneous medium fails to do). The success of Coulomb modeling depends on several factors, such as accurate data regarding the size and geometry of the main shock and aftershocks [*Steacy et al.*, 2004], the accuracy of earthquake data sets in general [*Kagan*, 2003] and knowledge of the regional crustal structure. Coulomb modeling might also benefit from a continuous reapplication of the modeling process with each aftershock, although this may not be practical in real time with large data sets. Irrespective of the mechanism at work, static stress triggering concepts are now being incorporated into probabilistic seismic hazard assessment. This model-dependant approach in turn requires detailed models for fault geometry and Earth structure which may not always be accurate, and which may lead to unwarranted complacency in zones of lowered Coulomb stresses.

[10] The work presented here tries instead to quantify properties of earthquake triggering statistically, without recourse to physical modeling of the underlying process. The advantage of such a method is that it requires no a priori assumptions about fault geometry or Earth structure, and hence may be used as a benchmark with which to test different physical hypotheses. As a natural progression of the global study carried out by *Huc and Main* [2003], we apply the method developed there to regional data sets, to look for spatial variations in the nature and scope of interearthquake triggering. We use a pair correlation technique, examining time and distance separations between epicenters of causally related events. It is applied to raw and time-randomized catalogues, to distinguish formally the triggered signal from the background seismicity. This is analogous to the separation of correlated and uncorrelated seismicity mentioned by *Helmstetter et al.* [2003].

[11] We initially examine triggering in and around Greece, to test the suitability of the method to smaller, bounded areas rather than the Earth as a whole. We then use Flinn-Engdahl seismic regions as boundaries for regional studies, to minimize subjectivity and also to allow our results to be compared with other work using the same system. This allows regional variations in the extent of triggering and earthquake diffusion to be calculated. Finally we look at the global data set for a range of magnitude thresholds, to compare the work here with that carried out previously on the CMT catalogue, and to examine how the triggering signal varies with magnitude.

[12] Carrying this method out for a range of time windows after each potential triggering event allows correlation lengths L and mean triggering distances $\langle r \rangle$ to be evaluated. Knowing how these parameters change over time means the temporal evolution of the spatial extent of triggered events can be determined. Analysis of this evolution, which can be fitted to a power law, allows us to calculate parameters that can be used as measure of the rate of diffusion of triggered events. The method can also be applied to determine the conditional probabilities for aftershock occurrence within a given distance and time after an earthquake in a direct way.

2. Method

[13] We used data from the International Seismological Centre (ISC) catalogue for the period 1 January 1964 to 31 December 2000. The catalogue was filtered to retain shallow events only (<70 km) with 4.5 m_b used as the magnitude threshold of completeness, leaving 91,199 events in the reduced catalogue. The analysis of a potential directional effect in triggering carried out by *Huc and Main* [2003] could not be repeated, as the ISC catalogue does not routinely report source orientation.

[14] To investigate the statistical properties of earthquake triggering, we begin by defining our null hypothesis that earthquakes are spatially clustered but temporally random. We treat each earthquake as a potentially triggering event, and every subsequent event as a potentially triggered event, thus making no a priori exclusions on what may be a triggered event [*Marsan et al.*, 1999; *Huc and Main*, 2003]. We then compare the original, unaltered data and deliberately time-randomized catalogues. This preserves the spatial clustering present in global seismicity, but allows us to look for any nonrandom temporal components in a clear and reproducible way.

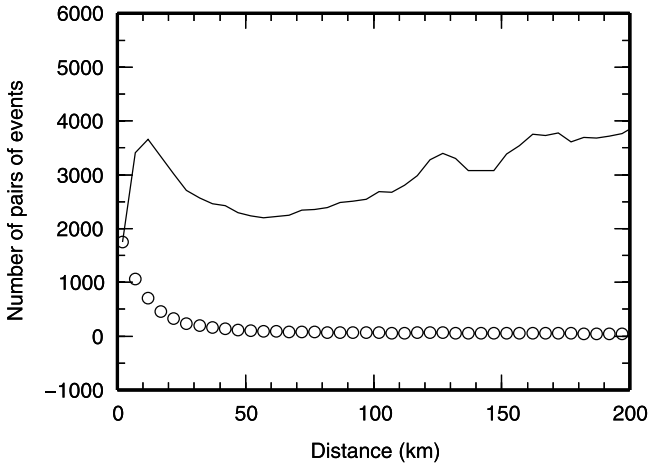

Figure 1. Plot showing the number of pairs of events following a potential triggering event as a function of distance. The raw histogram (solid line) shows an initial peak close to the triggering event, followed by a gradual rise attributable to the increasing area of successive annuli. The circles show the same histogram corrected for this area effect. The data are only shown to a maximum distance of 500 km, as the triggering effect is not seen at distances much greater than 200 km (data are from 2500 km radius around the Gulf of Corinth, for a time window of 1000 days).

[15] The method used is a form of pair correlation, where connections between pairs of events at positive time lag are analyzed. The difference in time and distance between each potential triggering/triggered pair are calculated, with the potential number of unique pairs N_P for a catalog of N_T events given by $N_P = (N_T^2 - N_T)/2$, assuming no prior knowledge of the spatial or temporal limits of any triggering effects. We calculate the time and distance separations for each trigger-triggered event pair, and then stack the data relative to the origin time of the trigger event. The result is a series of histograms of distance versus number of pairs, using 5 km bins, for a series of time windows ranging from 1 to 1000 days after the triggering event. The raw histograms are corrected to account for the increasing surface area in successive annuli, using a standard Euclidean normalization [*Lomnitz*, 1995]. An example is shown in Figure 1. All the histograms in this study used 5 km increments, finer than the previous global work due to the smaller length scales involved at lower-magnitude threshold.

[16] We then generate temporally random dates (random years, months and days separately) for the epicenters contained in the ISC catalogue, and sort the new catalogues chronologically. We create 20 such time-randomized catalogues, preserving the spatial distribution of seismicity, but removing any underlying temporal connections that could be attributed to interearthquake triggering. Histograms are then created for each of these 20 time-randomized catalogues in the same manner as the original data, and an average histogram is obtained for the null hypothesis of a Poisson process. Figure 2 shows these histograms after the area correction has been applied. We can now remove the background signal (as generated by the time-randomized catalogues) from the "real" signal, by subtracting the averaged histogram from the real data histogram. The actual physical triggering effect can then be interpreted to be the residual pair correlation function left after this subtraction. This method can be applied for a range of time windows to evaluate the time dependence.

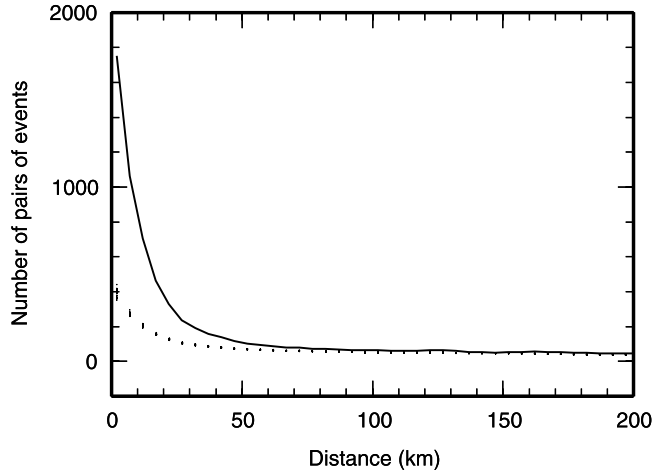

Figure 2. Area-corrected histogram from Figure 1 (solid line). Histograms for 20 time-randomized, area-corrected catalogues are shown as dots. The residual triggering signal is then taken to be the difference between the solid line and the average of the time-randomized data.

[17] The pair correlation function for the triggered events may be power law, an exponential, or a combination of both. Here we fit the data to the expression

$$N(r,t) = Ar^{-\alpha}e^{-r/L}, \tag{1}$$

where $N(r, t)$ is the number of pairs of events triggered at a distance $r \pm dr/2$ up to time t, A is the signal amplitude at unit distance (here 1 km), α is a power law exponent, and L is a correlation length (equivalent to the distance at which the triggering signal drops to $1/e$ of the value expected by extrapolation of the power law component). After normalization, equation (1) defines a conditional probability (Figure 3) for an event greater than the magnitude threshold

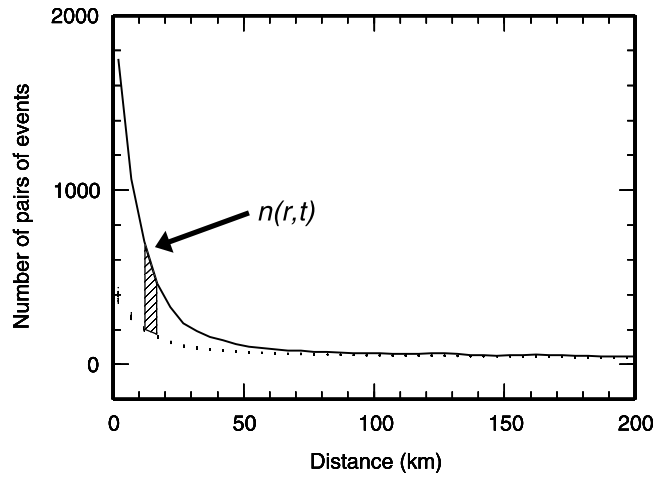

Figure 3. Application to time-dependent seismic hazard. $N(r, t)$ is calculated from the residual triggering signal. N_{CORR} is the total number of pairs under the solid line. $P(r, t)$ is the ratio of the two.

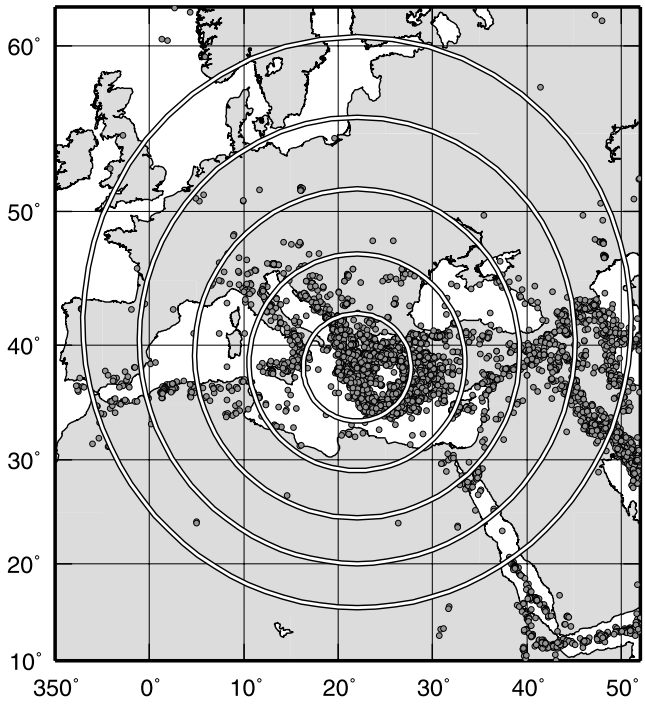

Figure 4. Map showing the areas and seismicity used for the initial regional study. Each circle is centered on 38°N, 22°E (the Gulf of Corinth). Radii are 500, 1000, 1500, 2000, and 2500 km, respectively.

being triggered within a given annulus up to a time t: $P(r, t) = N(r, t)/N_{CORR}$ (where N_{CORR} is the total number of pairs of events after the Euclidean area correction has been applied). This is useful in itself since it can be used directly for calculating time-independent hazard (for the average population), conditional on the occurrence of previous events above the magnitude threshold. The relative influence of the power law (short-range, $r \ll L$) and exponential (long-range, $r \sim L$) components of the distribution types can be determined from the data. Very long range triggering can then be defined for $r \gg L$.

[18] We also determine the mean triggering distance:

$$\langle r\rangle(t) = \sum_r \frac{rN(r,t)}{N(r,t)}, \qquad (2)$$

where $N(r, t)$ here is taken directly from the data, rather than a curve fit. Mean triggering distances are useful in that they are independent of any statistical model or regression technique. We then examine how L and $\langle r\rangle$ evolve with time by fitting them to power laws of the form:

$$L(t) = L_0(t/t_0)^H \qquad \langle r\rangle(t) = \langle r\rangle_0(t/t_0)^H, \qquad (3)$$

where L_0 and $\langle r\rangle_0$ are the correlation length and mean triggering distance, respectively for a minimum time $t = t_0$, which must be greater than or equal to the minimum time at which the catalogue can be regarded as complete. L_0 and $\langle r\rangle_0$ represent the "direct effect," or instantaneous response to the stress perturbation. The power law exponent H provides a quantitative measure of the rate of (directly and indirectly) triggered earthquake diffusion. The diffusion of triggered seismicity is in part controlled by the average properties of the percolation of stress outward from a triggering event, and as such H can also be thought of as an indicator of a (possibly stress related) diffusive process.

3. Results

3.1. Eastern Mediterranean

[19] The main aim of this case study was to determine the importance of finite sample boundaries in the analysis. We used circular regions to minimize the number of subjective parameters (to three, the origin and the radius). The origin was chosen to be 38°N, 22°E, and five concentric circles of radii r_{max} = 500, 1000, 1500, 2000, and 2500 km were defined (Figure 4). The method described in section 2 was then applied to each region for different time windows. The results from this first regional study are summarized in Table 1.

[20] For statistical stability the minimum time t_0 examined in this and the other regional studies was taken to be one day. An example of the residual pair correlation function $N(r,t)$ for r_{max} = 2500 km and t = 1, 10, 100 and 1000 days, together with the fits to equation (1), is shown on Figure 5. The amplitude increases systematically with time because the pair correlation function is integrated in time, but the trend is decelerating, indicating that triggering is a transient effect of finite duration. Meanwhile L increases from 9.63 to 13.28 km, indicating a relatively slow outward diffusion of epicenters relative to each other. The signal also drops to near zero at 100–150 km, indicating that on average, interearthquake triggering cannot at present be distinguished from background uncorrelated seismicity at distances greater than this.

[21] The residual correlation function of triggered events for t = 1000 days for each of the 5 circular regions is shown in Figure 6. Again, the amplitude and correlation length increase at a decreasing rate with increasing area size, and the detectable signal falls to near zero by 100–150 km. Each of the residual signals were fitted to equation (1), and used directly to determine $\langle r\rangle$ from equation (2) for a range of time windows. The resulting chi-square errors for equation (1) ranged from 0.0001 to 0.004, indicating a good fit to the data.

[22] The evolution of L and $\langle r\rangle$ over the time period 1–1000 days after an initial triggering event was determined for each value of r_{max}, and the results plotted in Figure 7.

Table 1. Summary of Results From Eastern Mediterranean Case Study[a]

Region Radius, km	Number of Events	$\langle r\rangle$		L	
		$\langle r\rangle_0$	H	L_0	H
500	1753	6.453	0.129	6.200	0.077
1000	3013	7.618	0.127	7.766	0.067
1500	3319	7.534	0.126	7.843	0.065
2000	3881	8.487	0.103	8.494	0.062
2500	4526	9.100	0.092	8.910	0.052

[a]Results from fitting $\langle r\rangle$ and L to a power law of form Ct^H (with C = $\langle r\rangle_0$ and L_0, respectively) for the first case study. The number of events in each region is also given. It can be seen that C rises in proportion to the area of each region and the number of events contained in each of those regions. H can in turn be seen to be inversely proportional to these two variables.

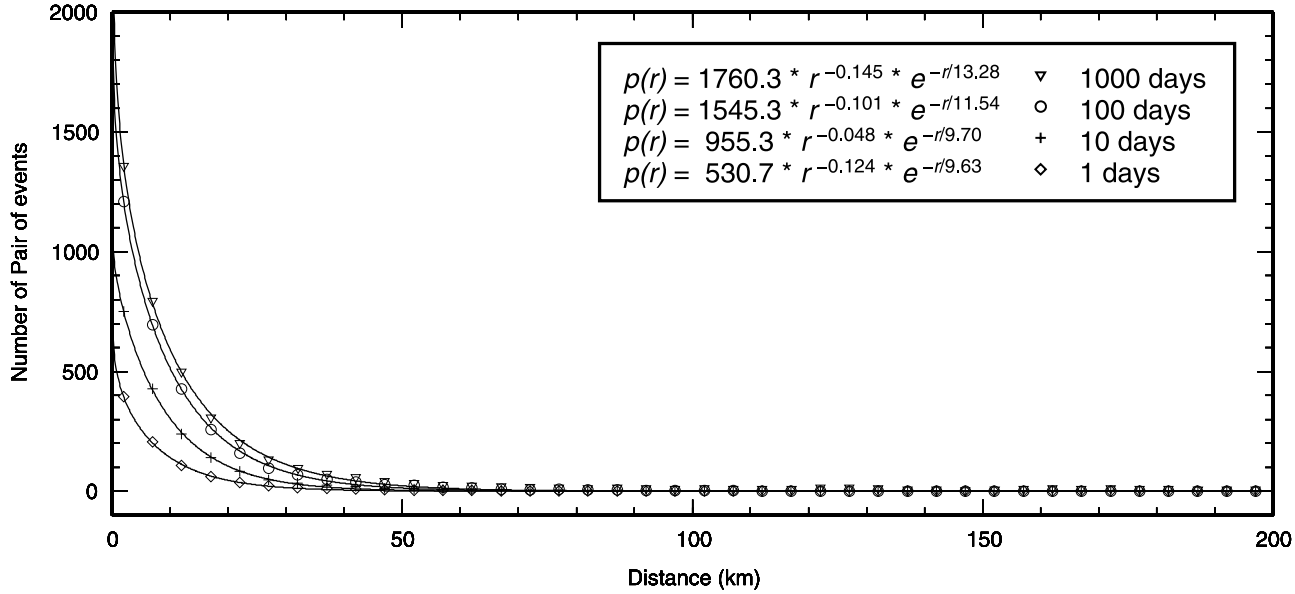

Figure 5. Residual triggering signals for the 2500 km radius region, for time windows of 1, 10, 100, and 1000 days. The signal can be seen to increase with time window. The fits to equation (1) are shown.

The larger study areas generally have a slightly greater value of $\langle r \rangle$ and L, but the trends on this graph are not strongly affected by r_{max}. In this sense finite size effects apparently are not of first-order importance, as long as the area used (as here) is at least twice as large as the maximum detectable extent of the triggering effect. Correlation lengths range from 7 to 15 km, increasing steadily over time. Mean triggering distances have a relatively flat trend between 1 and 100 days, but then appear to accelerate (on the log-log graph) to around 40 km by 1000 days as the triggering signal weakens. The diffusion exponent for t = 100 days was calculated from the slope on this log-log plot to be $H = 0.115 \pm 0.017$ for $\langle r \rangle$ and $H = 0.065 \pm 0.009$ for L.

3.2. Flinn-Engdahl Seismic Zones

[23] To extend the study to a range of tectonic environments, we applied the method to a range of Flinn-Engdahl seismic zones [*Flinn et al.*, 1974; *Young et al.*, 1996]. This removes any a posteriori subjectivity in choosing region boundaries, and will allow the results shown here to be compared to other studies using the same scheme. To preserve the statistical significance of the method, only

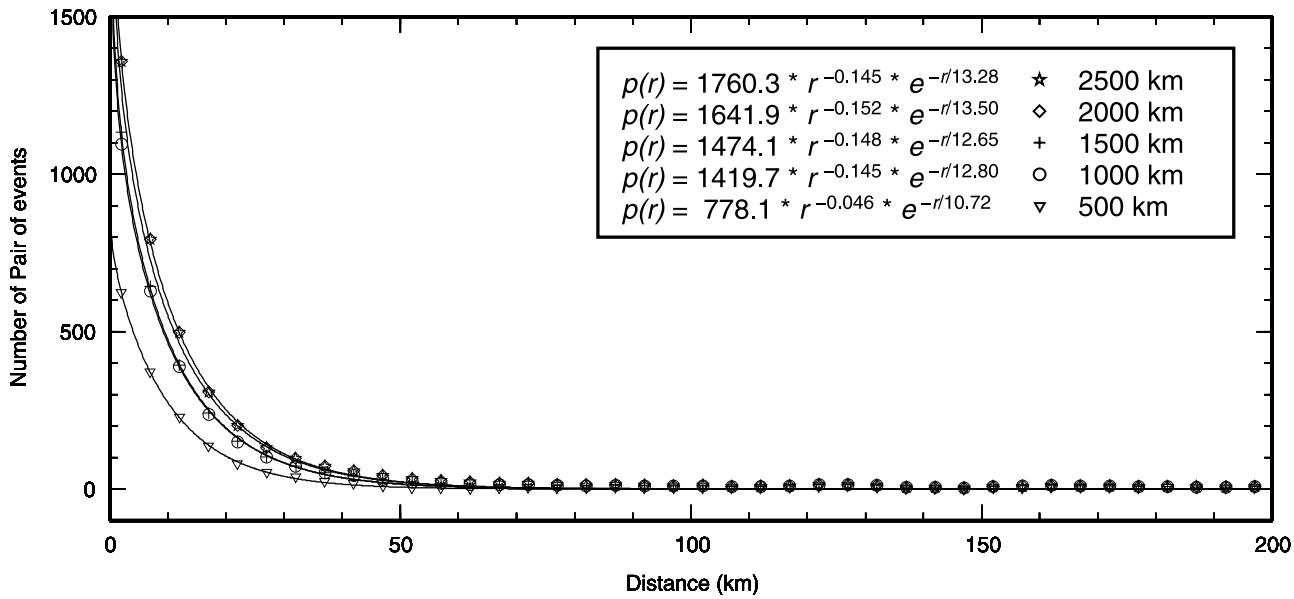

Figure 6. Residual triggering signals for each of the five circular regions used, over a time window of 1000 days. The signal here can be seen to be not strongly dependent on the area, increasing only slightly with area size. The fits to equation (1) are shown.

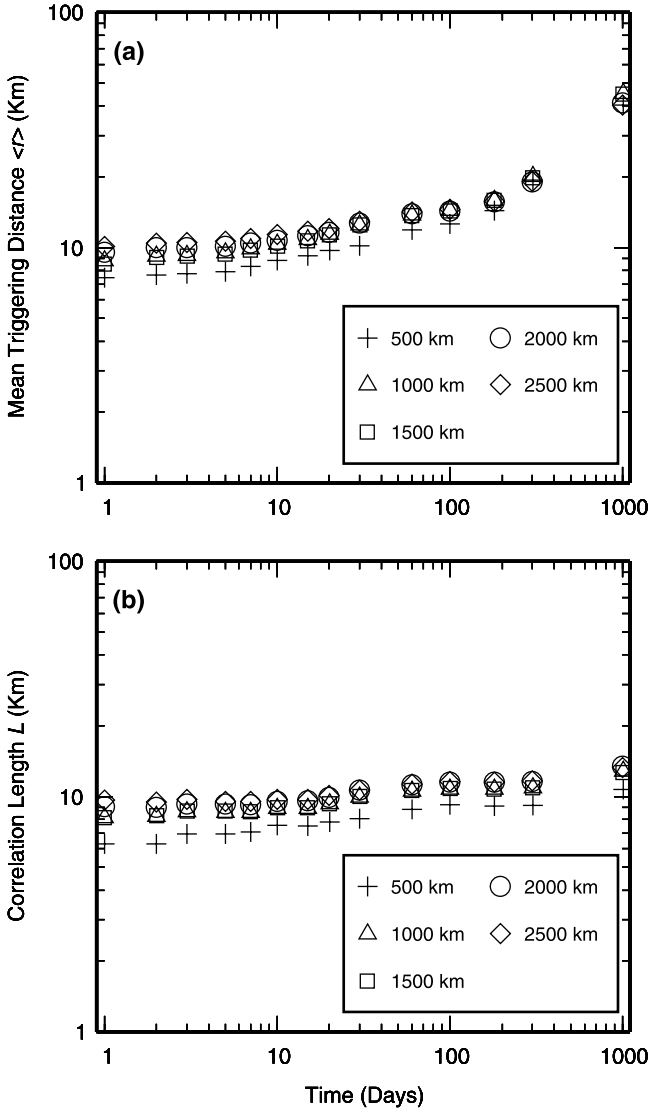

Figure 7. Summary of results from first regional study. (a) Plot of evolution of mean triggering distance $\langle r \rangle$ over time windows of 1–1000 days. (b) Plot of evolution of correlation length L over time.

regions with more than 1000 earthquakes were kept for further study. The 25 regions retained are numbered on Figure 8. A full list of the number of events in each and the type of region, as defined by *Kagan* [1997], is given in Table 2. This data constraint means that the sample is biased toward subduction zones (17 of the total) where most earthquakes occur. Of the remaining 8 regions, 3 are mid-ocean ridges, 3 are collision zones, 1 is an intraplate region, and 1 is classified by Kagan as "other." Again, we applied the same method using time windows after each potential trigger event of 1–1000 days. Correlation lengths and mean triggering distances were calculated and are shown grouped by region type in Figure 9, with mean triggering distances on the left and correlation lengths on the right.

[24] A quick visual inspection shows that $\langle r \rangle$ is typically greater than L for each region. The dominance of subduction zones means it is difficult to make comparisons between the tectonic regimes, but it is obvious that subduction zones have values of $\langle r \rangle$ and L greater than the other regions, ranging from 10 to 100 km. No other regions have values of either $\langle r \rangle$ or L greater than 40 km. Subduction zones appear to have a strongly bimodal distribution, with two clusters at $\langle r \rangle_0 \sim 10-15$ km, and $\langle r \rangle_0 \sim 20-30$ km. The diffusion exponents are in the range $H = 0.119 \pm 0.069$ for $\langle r \rangle$ and $H = 0.051 \pm 0.057$ for L.

[25] At times greater than 100–200 days, $\langle r \rangle$ appears to accelerate on the log-log plot for many of the zones. The same behavior is seen in some of the results for L. A similar trend to higher H at longer times was observed by *Marsan and Bean* [2003]. The transition to exponents H nearer 0.5 is likely to be due to a diffusive process that does not depend solely on cascading interevent triggering, such as the effect of viscoelastic stress transfer through the lower crust.

[26] The amplitude A from equation (1) varies with time (Figure 10a). The graph for each zone has the same asymptotic trend, with a slope dA/dt decreasing to near zero at 1000 days, indicative of a transient effect similar to that observed in global data by *Huc and Main* [2003]. The amplitude A is correlated to some extent with the total number of events in each region (Figure 10b). The power law exponents of equation (1) are clustered in Figure 11 around $\alpha = 0$, suggesting that the exponential component is dominant at a resolution of 5 km or so. The exponent α varies systematically between regions, but apart from a high degree of scatter at short times due to fewer pairs of events, it is remarkably invariant in time.

[27] Comparison of Figures 4 and 8 shows that the circular regions from the first case study cover some of the same area as Flinn-Engdahl zone 30. In fact, plotting $\langle r \rangle$ and L from each of these regions (Figure 12) reveals a very strong correlation between the two, despite the regions not being entirely coincident. This demonstrates that the actual shape of the region used does not exert a first-order influence on the results, as long as its size (short axis in this case) is greater than the maximum detectable triggering distance of ~150 km, which is the case for the Flinn-Engdahl seismic regions examined here. Also, it reinforces the idea that finite size effects brought about by using a bounded region are not overly important.

3.3. Global ISC Data

[28] We applied our method to the entire ISC data set, to compare our results with previous work on the global CMT catalogue by *Huc and Main* [2003]. Because of the greater number of data points in the global catalog, it is possible to examine the effect of the magnitude of threshold magnitude m_T (for triggering and triggered events). The global ISC catalogue was separated into 11 subcatalogues, with m_T ranging from 4.5 to 6.0. The number of events in each subset are listed in Table 3. Again due to the greater statistical stability brought by a larger data set we are able to reduce t_0 to 10^{-3} days. The resulting mean triggering distances and correlation lengths are plotted for the various magnitude thresholds in Figure 13. As before, mean triggering distances are systematically higher than correlation lengths. The mean triggering distances appear to be negatively correlated to the magnitude threshold, with $\langle r \rangle$ rising from a minimum of ~5 km to for $m_T = 6.0$ to ~10 km for $m_T = 4.5$. Fitting equations (3) to these data gives H to be close to 0.1.

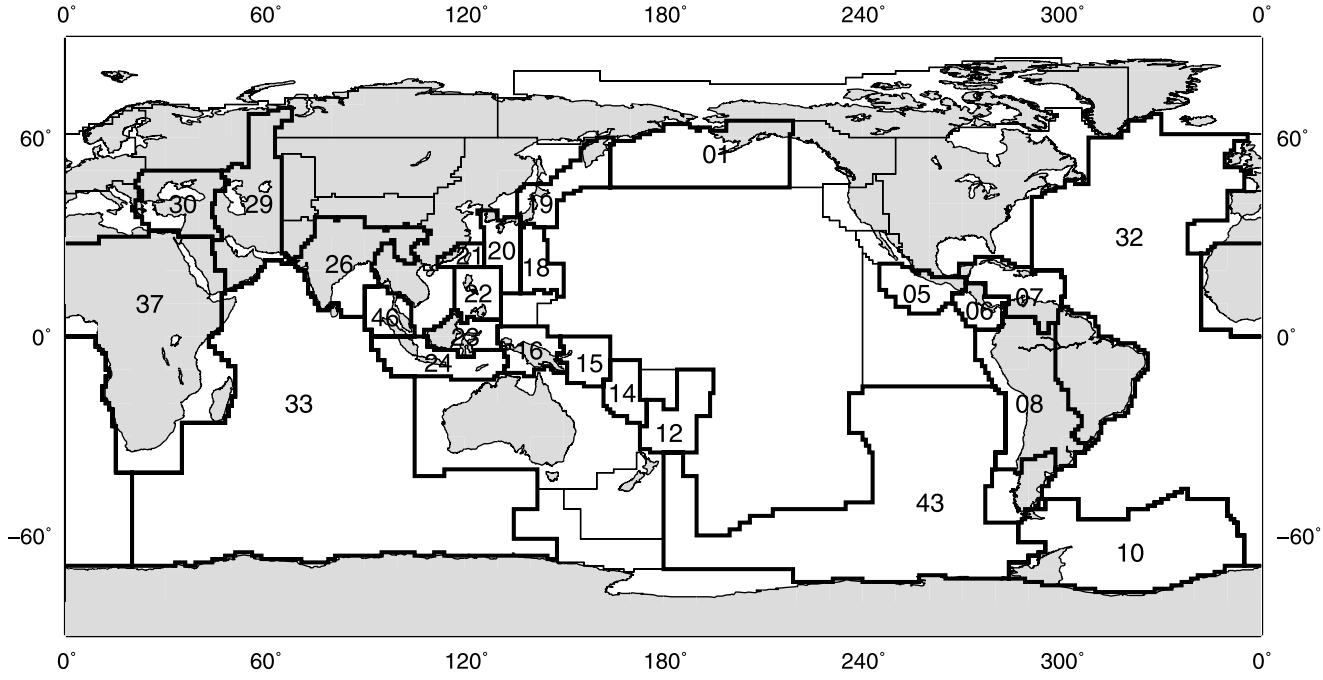

Figure 8. Map of Flinn-Engdahl seismic regions, with regions used in study outlined and numbered.

[29] The diffusion exponent H for each threshold varies for $\langle r \rangle$ from −0.049 for $m_T = 6.0$ data to 0.133 for $m_T = 5.1$. Similar results can be seen for the correlation lengths, but break down somewhat at the higher-magnitude thresholds and shorter time separations due to a lack of events in the catalogues. For example, the data set for $m_T = 6.0$ contains only 678 earthquakes spread over the entire globe. Fitting such noisy data to equation (1) appears to be unstable above magnitude thresholds of 5.0 m_b. Below 5.0 m_b, the results show trends similar to those seen in the regional studies of $\langle r \rangle$, but again of lower amplitude. Mean triggering distances range from 10 to 25 km, similar to those observed by *Huc and Main*

Table 2. Summary of Results From Flinn-Engdahl Case Study[a]

				$\langle r \rangle$		L	
F-E	Region Name	Number of Events	Region Type	$\langle r \rangle_0$	H	L_0	H
1	Alaska-Aleutian Arc	5585	subduction	57.716	0.037	70.308	0.050
5	Mexico-Guatemala	2013	subduction	20.438	0.129	20.482	0.088
6	Central America	1775	subduction	26.346	0.112	27.192	0.089
7	Caribbean Loop	1133	subduction	14.817	0.034	15.419	0.011
8	Andean South America	4119	subduction	23.457	0.057	20.542	0.069
12	Kermadec-Tonga-Samoa Basin	6489	subduction	21.879	0.192	17.848	0.169
14	Vanuatu Islands	4140	subduction	19.309	0.116	19.879	0.074
15	Bismarck-Solomon Islands	4308	subduction	22.748	0.128	20.700	0.119
16	New Guinea	3416	subduction	22.633	0.123	25.311	0.028
18	Guam-Japan	2734	subduction	13.199	0.099	11.671	0.073
19	Japan-Kamchatka	10187	subduction	28.460	0.062	33.991	0.012
20	SE Japan-Ryukyu Islands	1420	subduction	9.275	0.189	17.610	0.000
21	Taiwan	1664	subduction	14.465	0.066	14.179	0.009
22	Philippines	4552	subduction	17.384	0.138	18.354	0.084
23	Borneo-Sulawesi	3553	subduction	6.024	0.319	8.475	0.141
24	Sunda Arc	3451	subduction	25.845	0.176	35.031	0.124
46	Andaman Islands-Sumatera	1028	subduction	11.701	0.136	13.661	0.020
26	India-Xizand-Sichuan-Yunnan	1555	collision	6.263	0.141	8.773	0.033
29	Western Asia	2212	collision	11.094	0.097	9.393	0.003
30	Middle East-Crimea-Balkans	2657	collision	6.101	0.237	7.419	0.047
37	Africa	1039	intracontinental	13.506	0.013	9.582	0.032
32	Atlantic Ocean	3519	mid-ocean ridge	9.448	0.132	8.523	0.045
33	Indian Ocean	2832	mid-ocean ridge	17.304	0.085	16.325	0.020
43	SE and Antarctic Pacific Ocean	1596	mid-ocean ridge	14.696	0.029	16.586	−0.118
10	Southern Antilles	1619	other	11.641	0.135	10.155	0.055

[a]Results from fitting $\langle r \rangle = \langle r \rangle_0 (t/t_0)^H$ for the mean triggering distances and $L = L_0 (t/t_0)^H$ for the correlation lengths from the Flinn-Engdahl case study. Regions are grouped by types put forward by *Kagan* [1997].

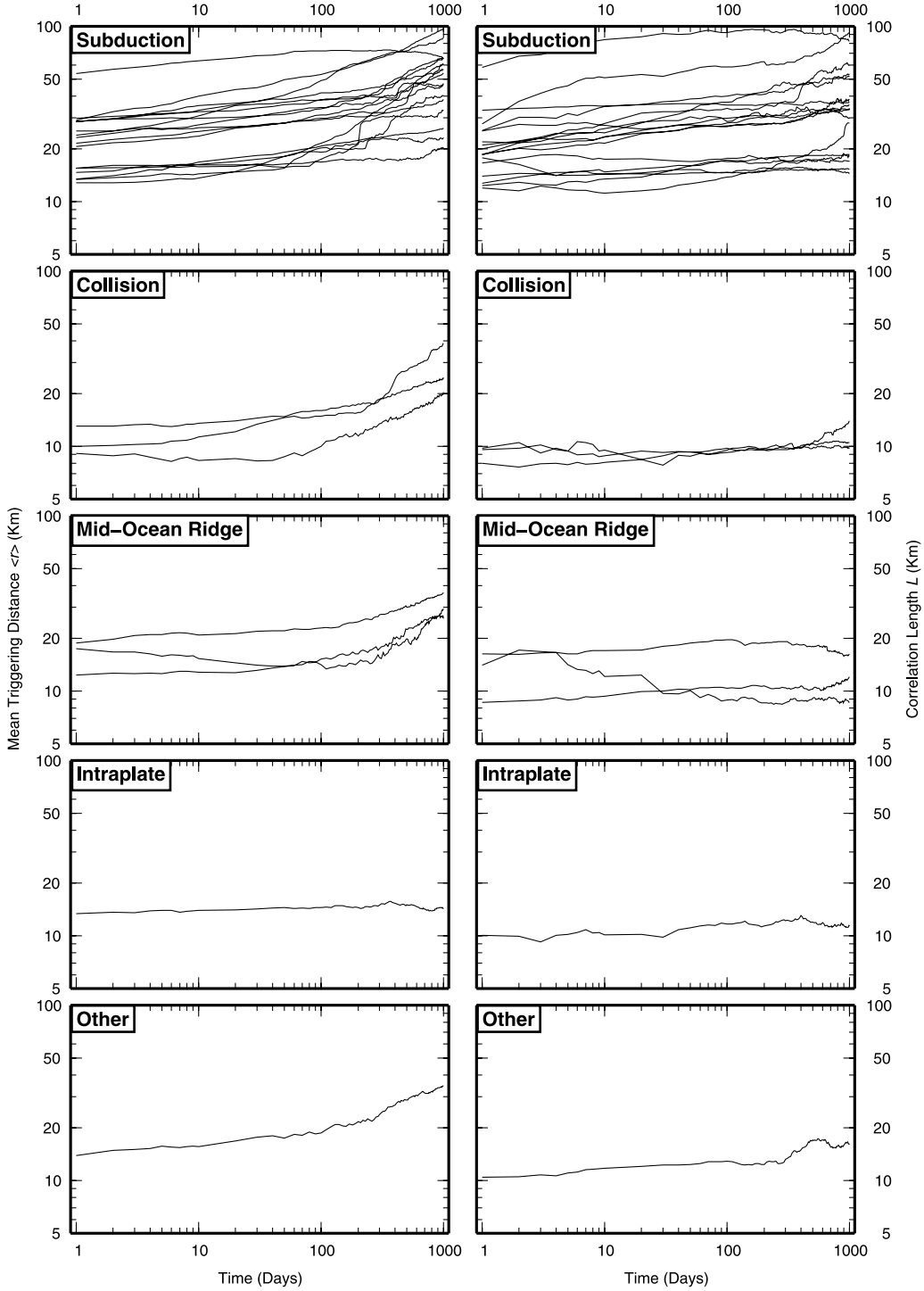

Figure 9. Plot of (left) mean triggering distances $\langle r \rangle$ and (right) correlation lengths L for the Flinn-Engdahl seismic regions, grouped by tectonic region type.

[2003]. At times greater than ~400 days a slight increase in H can be seen, consistent with that also seen in many of the regional studies.

4. Discussion

[30] In all of the cases studied, we found that interearthquake triggering cannot be distinguished from background seismicity at distances greater than 150 km or so, consistent with the results of *Huc and Main* [2003] and *Gasperini and Mulargia* [1989]. This means that either (1) such events are too rare to be seen above the noise at present or (2) an equal number of potential events are being "clock retarded" in stress shadows. The first hypothesis should be disproven before preferring the second. The absence (on average) of very long range triggering is consistent with earthquakes being triggered predominantly by static stress changes which do not operate over long distances [*Gomberg et al.*,

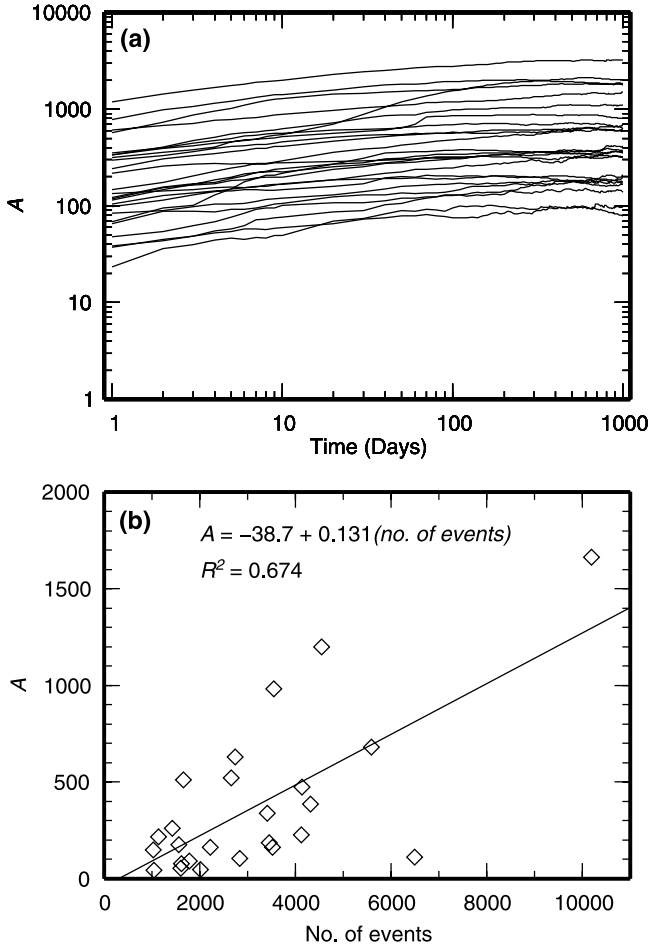

Figure 10. (a) Evolution of A, from equation (1), over time. The trends of the lines are similar, varying mainly in amplitude. (b) A moderate positive correlation between the number of events in each zone and the amplitude of A.

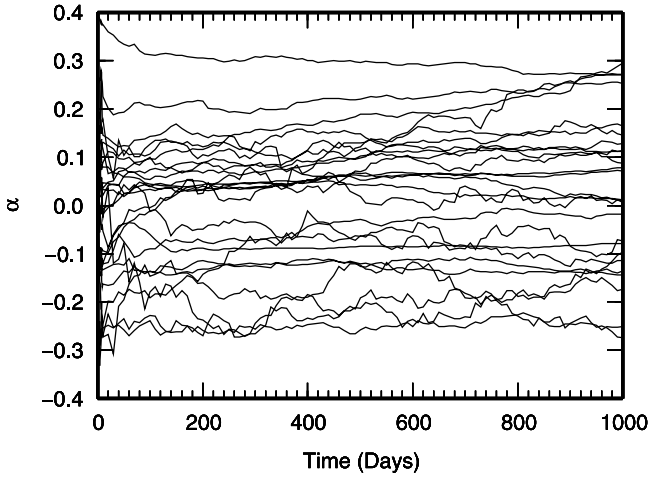

Figure 11. Plot showing variation of α, the power law component from equation (1), over time for each of the F-E zones. The values of α are generally small and near zero, meaning that the pair correlation function could be approximated well by an exponential term only.

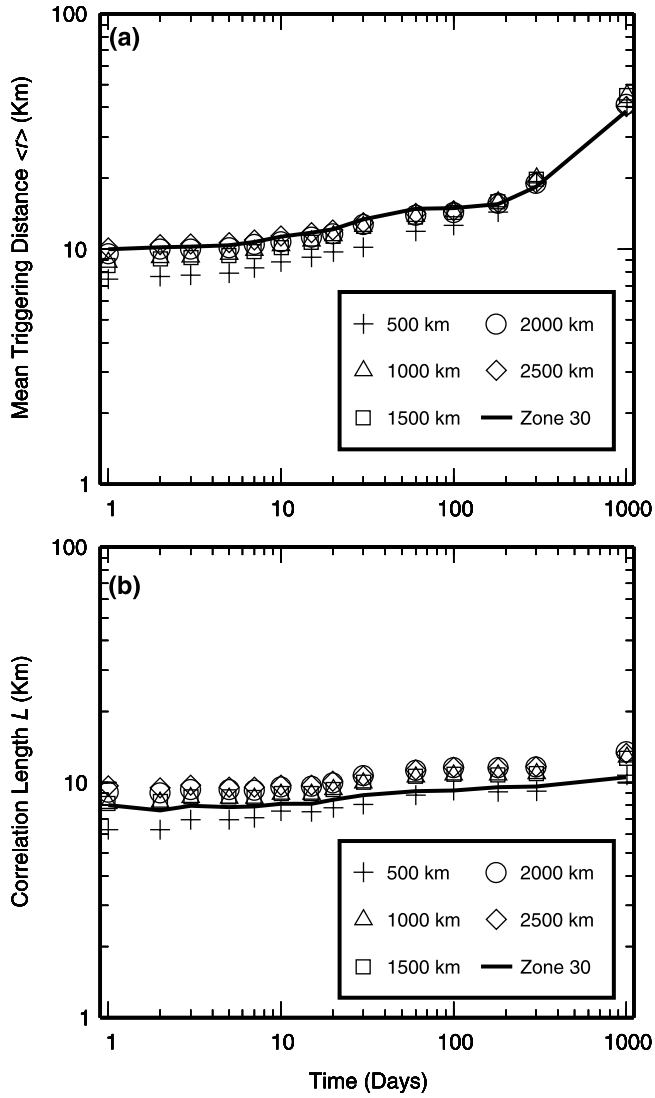

Figure 12. A plot of the results shown in Figure 6, but with evolution of mean triggering $\langle r \rangle$ and correlation lengths L from Flinn-Engdahl seismic region 30 (Middle East–Crimea–Balkans) overlain. It can be seen that the results from each of the areas correspond closely, despite there being a discrepancy in the boundaries used. This shows that the method is not strongly affected by the area chosen, and edge effects are not overly important.

1998]. Our results do not preclude some individual events being triggered at very long range by dynamic effects, but such events must be relatively rare compared to the background noise.

[31] Our correlation lengths are of similar orders of magnitude to those of *Huc and Main* [2003]. For the two regional studies, L is typically of the order of 10–40 km, rising to 100 km in some subduction zones. These values are comparable in size to the thickness of the seismogenic zone. Notably, we would expect subduction zones to have a deeper brittle-plastic transition due to the cooling effect of the descending slab [*Schubert et al.*, 1975], consistent with the results presented here.

[32] The method appears to be relatively robust with respect to choice of study area. In the case of the five

Table 3. Results From Global ISC Case Study[a]

Magnitude Threshold	Number of Events	$\langle r \rangle$		L	
		$\langle r \rangle_0$	H	L_0	H
4.5	99119	22.32	0.101	18.53	0.071
4.6	77750	21.23	0.117	17.82	0.076
4.7	64490	20.37	0.118	17.16	0.074
4.8	51758	19.46	0.121	16.70	0.073
4.9	40198	18.42	0.123	15.77	0.077
5.0	23002	17.78	0.126	15.04	0.076
5.1	16968	16.15	0.133	13.95	0.080
5.2	12447	16.08	0.123	15.16	0.056
5.3	9003	15.34	0.119	13.91	0.070
5.4	6426	13.99	0.114	11.82	0.080
5.5	4629	14.75	0.096	11.62	0.031
5.6	3268	14.09	0.074	9.59	0.035
5.7	2317	12.84	0.064	7.76	0.032
5.8	1564	12.97	0.044	10.13	−0.032
5.9	1064	11.01	0.016	8.69	−0.042
6.0	678	12.12	0.065	8.14	−0.049

[a]Results from power law fitting to $\langle r \rangle$ and L for global catalogue, for a range of magnitude thresholds from 4.5 to 6.0 m_b.

circular regions centered on the Gulf of Corinth, the largest has over twice as many events, spread over a much larger area than the smallest one. However, the evolution of $\langle r \rangle$ and L for both are very similar. The results from Flinn-Engdahl zone 30 also correlate very well with these results, despite being not totally coincident with the circular regions. We believe this can be attributed to our choice of study zones being large compared to the detectable range of influence.

[33] The correlation length and mean triggering distance have comparable values, but found L is generally less that $\langle r \rangle$, in contrast to that of *Huc and Main* [2003]. We also found a transition to more rapid diffusion at the longer times investigated here (300–1000 days).

[34] In the global catalogue we found that mean triggering distances, which range from 5 to 50 km, tend to decrease weakly with magnitude threshold (Figure 13), in contrast to the work by *Huc and Main* [2003, Figure 6], where $\langle r \rangle$ increases weakly with magnitude threshold. Our results, at lower-magnitude threshold, imply that the greater proportion of "receiver" earthquakes may dominate the signal, with smaller events being easier to trigger at larger distances. If $\langle r \rangle$

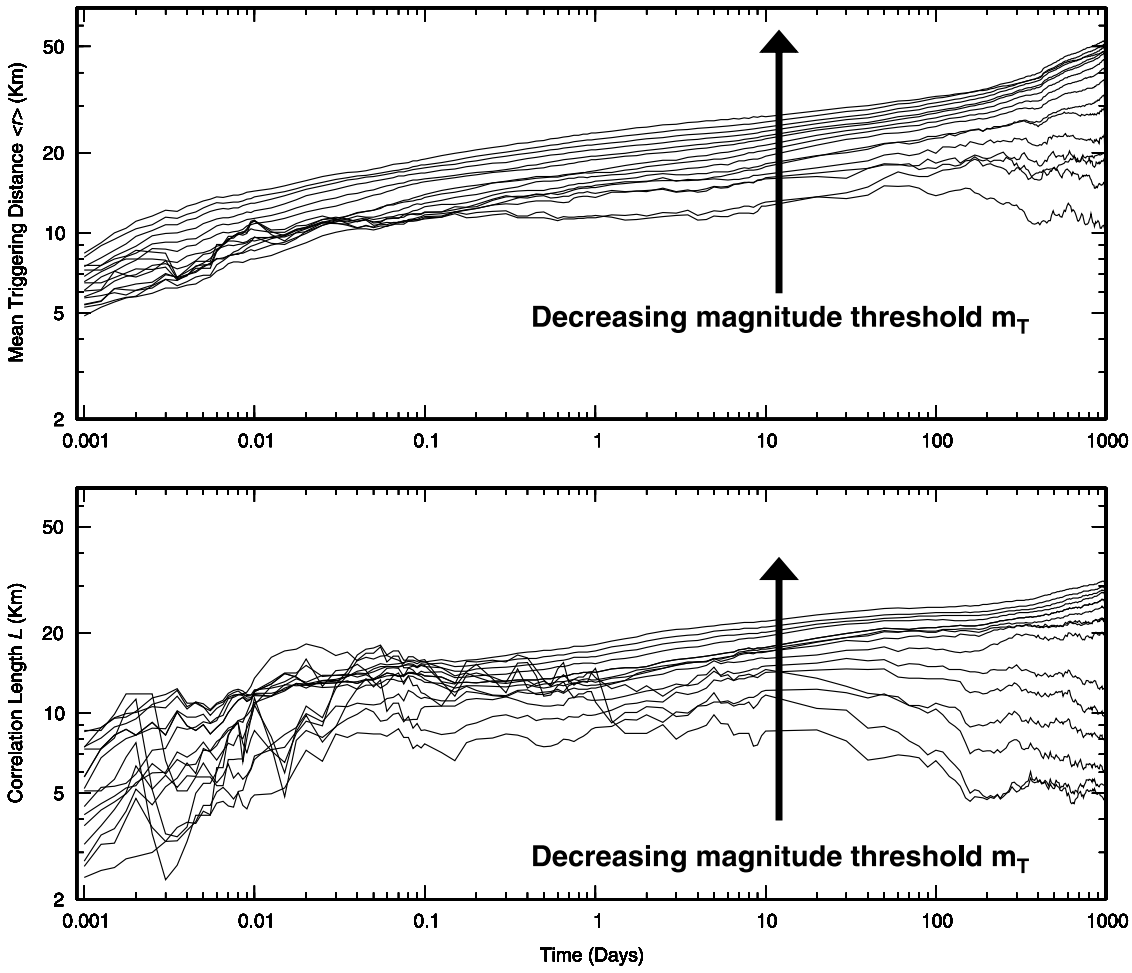

Figure 13. Plot of global results for $\langle r \rangle$ and L, over 1–1000 days, for magnitude thresholds m_T from 4.5 to 6.0. Subsets with lower-magnitude thresholds (and hence more events) have higher values of $\langle r \rangle$ and L. The diffusion signals are more scattered at higher-magnitude thresholds and for smaller time windows, where the number of pairs of events drops off.

is relatively insensitive, or even independent of magnitude threshold (e.g., as in the work by *Felzer et al.* [2004]) then correlation length must be determined a priori by factors other than the triggering magnitude threshold, most likely the seismogenic thickness. The correlation length may also appear to decrease with time if the magnitude threshold is too high (Figure 13), most likely due to statistical instability associated with having fewer pairs of events. Similarly at shorter times there is greater scatter in the data, also due to the lack of potential triggering-triggered pairs. The results of Figure 13 also show similar effects for $\langle r \rangle$ but to a lesser degree, implying that $\langle r \rangle$ is more robust than model-dependent parameters such as L.

[35] The mean triggering distance at a given time is relatively insensitive to the magnitude threshold, at least up to magnitude 6 or so (Figure 13). Such an event would have a source dimension comparable to the seismogenic thickness. For trigger magnitude thresholds much greater than this we may expect correlation lengths along strike to exceed those found here, due to the fact that the source dimension is greater than the seismogenic thickness. With current data it is not possible to test this hypothesis. Again it is important to emphasis that we have plotted the statistical average of the population as a function of the completeness threshold, and not the response of the earth to a triggering event of a specific magnitude.

[36] For the eastern Mediterranean study $H = 0.115 \pm 0.017$ for $\langle r \rangle$ and $H = 0.065 \pm 0.009$ for $\langle r \rangle$ L, with $m_T = 4.5$. For the Flinn-Engdahl regions, we find $H = 0.119 \pm 0.069$ and $H = 0.051 \pm 0.057$ for $m_T = 4.5$. In the case of the global catalogs, $H = 0.049 \pm 0.047$ and $H = -0.026 \pm 0.090$, again calculated from $\langle r \rangle$ and L, respectively. The low values of H are consistent with the work by *Marsan et al.* [2000], who found H to be 0.1 for mining-induced seismicity, and 0.22 at the Long Valley caldera and in southern California. *Marsan and Bean* [2003] calculated H at a global scale (for the Council of the National Seismic System catalogue, 1963–1998, $M \geq 5$, depth ≤ 70 km) to be bimodal. For times spanning 10^{-3} to 10 days, $H = 0.19$, and for times over the range 10 to 10^3 days, H was shown to be 0.4, significantly higher than any values of H derived here. They found H to be 0.37 for ocean ridges, higher by more than 0.2 compared to those listed in Table 2. They also report a positive correlation between heat flow and H, suggesting a strong thermal control (consistent in turn with seismogenic depth being a strong determinant of correlation length, since low heat flow leads to a deeper brittle/ductile transition). Comparing physical parameters such as heat flow, crustal thickness, or relative plate velocities would be a natural progression of the regional analysis presented here but with current data would require either narrowing the size of the zones to the correlation length of heat flow data (thereby reducing the statistical stability) or a major coarse graining of data to match the size of the F-E zones (reducing the resolution).

[37] *Helmstetter et al.* [2003] calculated values of H for 21 main shock sequences in California, using two methods to remove the background, or uncorrelated, seismicity. For the first method, using a windowing technique, they found H ranging between 0.01 and 0.41, with a mean of 0.08 ± 0.09, similar to the range reported here. Their second technique (using a wavelet method to remove the uncorrelated seismicity) produced values of H ranging between -0.09 and 0.24, with a mean of 0.03 ± 0.09. It is clear that the initial diffusion of seismic activity is very slow, possibly explained by the dominant effect of preexisting correlation lengths, where triggered events tend to localize on preexisting fault networks.

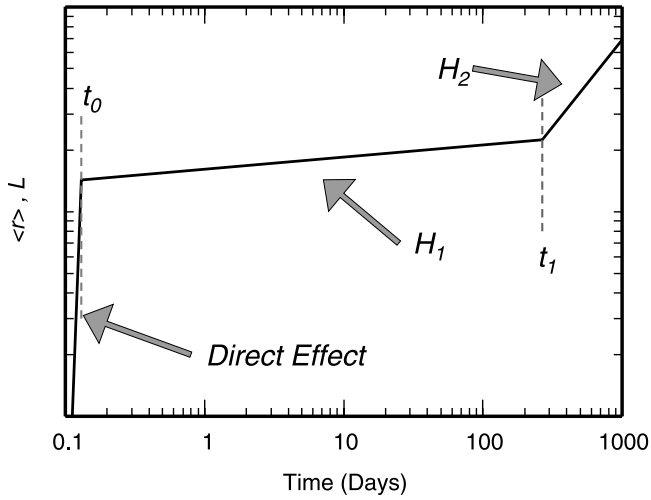

Figure 14. Diagram of three proposed regimes for stress transfer. The direct effect is the instantaneous response to the stress perturbation following an earthquake. H_1 is the diffusion process, and H_2 describes a longer-term process, possibly viscoelastic stress transfer in the lower ductile crust. The time t_1 where H_2 overtakes H_1 appears to occur at $\sim$100 days.

[38] An increased diffusion exponent at longer times implies a three-stage model may be required to explain the data (Figure 14), of the form

$$\begin{aligned} \log L &= \log L_0 + H_1 \log(t/t_0) \quad t_0 < t < t_1 \\ \log L &= \log L_1 + H_2 \log(t/t_1) \quad t > t_1. \end{aligned} \tag{4}$$

The first part (L_0) represents the short-term or "direct effect," the instantaneous response to the stress perturbation following an earthquake. After time t_0, as described in section 2, we then expect a slow diffusion process as reported here and in previous work, consistent with primary or secondary triggering involving threshold dynamics. This is consistent with the purely statistical epidemic-type aftershock sequence (ETAS) model [*Helmstetter et al.*, 2003], but does not preclude physical models such as rate-and-state friction [*Dieterich*, 1994] or stress corrosion cracking as quantitative explanations for the data presented here. After a later time t_1, we see an increase in H. Again, this could be a combination of effects due to several physical processes. One possible mechanism would be a longer-range stress transfer process, such as viscoelastic deformation of the lower crust. A similar increase in the diffusion exponent has also been observed in global data by *Marsan and Bean* [2003].

5. Conclusions

[39] We confirm that no significant triggering signal is seen above the noise beyond $\sim$150 km. A large data set with a

lower threshold of completeness has allowed us to apply our method to different tectonic regimes. The residual triggering signals, to which equation (1) is fitted, determine a probability distribution of triggered events conditional on the occurrence of a triggering event. As such they could be used after appropriate normalization as estimates of conditional probabilities for time-dependant seismic hazard as an average for the population as a whole. Correlation lengths L and mean triggering distances $\langle r \rangle$ are found to be on the order of 10–40 km in most cases, with the exception of subduction zones, where they range over 10–100 km. This may be due to variations in seismogenic thickness; for example, rapidly descending subduction zones will have a deeper brittle-ductile transition due to thermal cooling. Subduction zones display a bimodal distribution in L and $\langle r \rangle$.

[40] Our values of $\langle r \rangle$ and L are higher than those derived at higher-magnitude threshold from the CMT catalog. Exponents determined from $\langle r \rangle$ are generally larger than when calculated from L. For the eastern Mediterranean $H = 0.115 \pm 0.017$ for $\langle r \rangle$ and $H = 0.065 \pm 0.009$ for L. For the Flinn-Engdahl case study $H = 0.119 \pm 0.069$ for $\langle r \rangle$ and $H = 0.051 \pm 0.057$ for $\langle L \rangle$. For the global catalogs, $H = 0.049 \pm 0.047$ for $\langle r \rangle$ and $H = -0.026 \pm 0.090$ for L. All are much lower than 0.5, the value for a homogenous Fickian diffusion process, implying strong preexisting crustal heterogeneity. The values of H for the global study tend to be smaller than those calculated by *Huc and Main* [2003] from the CMT catalog ($0.05 < H < 0.06$). The global values of $\langle r \rangle$ and L show a systematic increase with decreasing magnitude threshold, implying smaller events may be easier to trigger.

[41] **Acknowledgments.** This work was funded by NERC Studentship NER/S/A/2001/06166 and also in part by the Corinth Rift Laboratory (http://www.Corinth-rift-lab.org), a European Union funded project. We thank Associate Editor Massimo Cocco, Frank Evans and two anonymous reviewers for their constructive and detailed reviews, and Bruce Malamud for comments during the course of the work.

References

Brodsky, E. E., E. Roeloffs, D. Woodcock, I. Gall, and M. Manga (2003), A mechanism for sustained groundwater pressure changes induced by distant earthquakes, *J. Geophys. Res.*, *108*(B8), 2390, doi:10.1029/2002JB002321.

Dieterich, J. (1994), A constitutive law for rate of earthquake production and its application to earthquake clustering, *J. Geophys. Res.*, *99*(B2), 2601–2618.

Felzer, K. R., T. W. Becker, R. E. Abercrombie, G. Ekström, and J. R. Rice (2002), Triggering of the 1999 M_W 7.1 Hector Mine earthquake by aftershocks of the 1992 M_W 7.3 Landers earthquake, *J. Geophys. Res.*, *107*(B9), 2190, doi:10.1029/2001JB000911.

Felzer, K. R., R. E. Abercrombie, and G. Ekstrom (2003), Secondary aftershocks and their importance for aftershock forecasting, *Bull. Sesimol. Soc. Am.*, *93*, 1433–1448.

Felzer, K. R., R. E. Abercrombie, and G. Ekstrom (2004), A common origin for aftershocks, foreshocks, and multiplets, *Bull. Sesimol. Soc. Am.*, *94*, 88–98.

Flinn, E. A., E. R. Engdahl, and A. R. Hill (1974), Seismic and geographical regionalization, *Bull. Seismol. Soc. Am.*, *64*, 771–993.

Gasperini, P., and F. Mulargia (1989), A statistical analysis of seismicity in Italy: The clustering properties, *Bull. Seismol. Soc. Am.*, *79*, 973–988.

Gomberg, J., N. M. Beeler, M. L. Blanpied, and P. Bodin (1998), Earthquake triggering by transient and static deformations, *J. Geophys. Res.*, *103*(B10), 24,411–24,426.

Harris, R. A., and R. W. Simpson (1998), Suppression of large earthquakes by stress shadows: A comparison of Coulomb and rate-and-state failure, *J. Geophys. Res.*, *103*(B10), 24,439–24,451.

Harris, R. A., R. W. Simpson, and P. A. Reasenberg (1995), Influence of static stress changes on earthquake locations in southern California, *Nature*, *375*, 221–224.

Helmstetter, A., G. Ouillon, and D. Sornette (2003), Are aftershocks of large Californian earthquakes diffusing?, *J. Geophys. Res.*, *108*(B10), 2483, doi:10.1029/2003JB002503.

Hill, D. P., et al. (1993), Seismicity remotely triggered by the magnitude 7.1 Landers, California, earthquake, *Science*, *260*, 1617–1623.

Huc, M., and I. G. Main (2003), Anomalous stress diffusion in earthquake triggering: Correlation length, time dependence, and directionality, *J. Geophys. Res.*, *108*(B7), 2324, doi:10.1029/2001JB001645.

Kagan, Y. Y. (1997), Seismic moment-frequency relation for shallow earthquakes: Regional comparison, *J. Geophys. Res.*, *102*(B2), 2835–2852.

Kagan, Y. Y. (2003), Accuracy of modern global earthquake catalogs, *Phys. Earth Planet. Inter.*, *135*, 173–209.

Kagan, Y. Y., and D. D. Jackson (1998), Spatial aftershock distribution: Effect of normal stress, *J. Geophys. Res.*, *103*(B10), 24,453–24,467.

King, G. C. P., R. S. Stein, and J. Lin (1994), Static stress changes and the triggering of earthquakes, *Bull. Seismol. Soc. Am.*, *84*, 935–953.

Lomnitz, C. (1995), On the distribution of distances between random points on a sphere, *Bull. Seismol. Soc. Am.*, *85*, 951–953.

Lomnitz, C. (1996), Search of a worldwide catalog for earthquakes triggered at intermediate distances, *Bull. Seismol. Soc. Am.*, *86*, 293–298.

Marsan, D. (2003), Triggering of seismicity at short timescales following Californian earthquakes, *J. Geophys. Res.*, *108*(B5), 2266, doi:10.1029/2002JB001946.

Marsan, D., and C. J. Bean (2003), Seismicity response to stress perturbations, analysed for a world-wide catalogue, *Geophys. J. Int.*, *154*, 179–195.

Marsan, D., C. J. Bean, S. Steacy, and J. McCloskey (1999), Spatio-temporal analysis of stress diffusion in mining induced seismicity, *Geophys. Res. Lett.*, *26*, 3697–3700.

Marsan, D., C. J. Bean, S. Steacy, and J. McClosky (2000), Observation of diffusion processes in earthquake populations and implications for their predictability of seismicity systems, *J. Geophys. Res.*, *105*(B12), 28,081–28,094.

Melini, D., A. Casarotti, A. Piersanti, and E. Boschi (2002), New insights on long range fault interactions, *Earth Planet. Sci. Lett.*, *204*, 363–372.

Parsons, T. (2002), Global Omori law decay of triggered earthquakes: Large aftershocks outside the classical aftershock zone, *J. Geophys. Res.*, *107*(B9), 2199, doi:10.1029/2001JB000646.

Schubert, G., D. A. Yuenm, and D. L. Turcotte (1975), Role of phase transitions in a dynamic mantle, *Geophys. J. R. Astron. Soc.*, *42*(2), 705–735.

Steacy, S., D. Marsan, S. S. Nalbant, and J. McCloskey (2004), Sensitivity of static stress calculations to the earthquake slip distribution, *J. Geophys. Res.*, *109*, B04303, doi:10.1029/2002JB002365.

Stein, R. S., G. C. P. King, and J. Lin (1994), Stress triggering of the 1994 $M = 6.7$ Northridge, California, earthquake by its predecessors, *Science*, *265*, 1432–1435.

Toda, S., R. S. Stein, P. A. Reasenberg, and J. H. Dieterich (1998), Stress transferred by the $M_w = 6.9$ Kobe, Japan, shock: Effect on aftershocks and future earthquake probabilities, *J. Geophys. Res.*, *103*(B10), 24,543–24,565.

Utsu, T., Y. Ogata, and S. Matsu'ura (1995), The centenary of the Omori formula for a decay law of aftershock activity, *J. Phys. Earth.*, *43*, 1–33.

Young, J. B., B. W. Presgrave, H. Aichele, D. A. Wiens, and E. A. Flinn (1996), The Flinn-Engdahl regionalization scheme: The 1995 revision, *Phys. Earth Planet. Inter.*, *96*, 223–297.

I. G. Main and C. McKernon, School of GeoSciences, University of Edinburgh, West Mains Road, Edinburgh, Midlothian EH9 3JW, UK. (ian.main@glg.ed.ac.uk; conor.mckernon@glg.ed.ac.uk)